

CONFIRMATION OF A STEEP LUMINOSITY FUNCTION FOR Ly α EMITTERS AT $z = 5.7$: A MAJOR COMPONENT OF REIONIZATION*

ALAN DRESSLER

Carnegie Observatories, 813 Santa Barbara St., Pasadena, California 91101-1292

ALAINA HENRY

Astrophysics Science Division, Goddard Space Flight Center, Code 665, Greenbelt, MD 20771

CRYSTAL L. MARTIN

University of California, Santa Barbara, Department of Physics, Santa Barbara, CA 93106

MARCIN SAWICKI

St. Mary's University, Department of Astronomy and Physics, 923 Robie Street, Halifax, N.S., B3H 3C3, Canada

PATRICK MCCARTHY

Carnegie Observatories, 813 Santa Barbara Street, Pasadena, California 91101-1292

EDWARD VILLANEUVA

Carnegie Observatories, 813 Santa Barbara Street, Pasadena, California 91101-1292

Submitted: 2014 September 15; accepted: 2015 April 11

ABSTRACT

We report the first direct and robust measurement of the faint-end slope of the Ly- α emitter (LAE) luminosity function at $z = 5.7$. Candidate LAEs from a low-spectral-resolution blind search with IMACS on Magellan-Baade were targeted at higher resolution to distinguish high redshift LAEs from foreground galaxies. All but 2 of our 42 single-emission-line systems have flux $F < 2.0 \times 10^{-17}$ ergs s⁻¹ cm⁻², making these the faintest emission-lines observed for a $z = 5.7$ sample with known *completeness*, an essential property for determining the faint end slope of the LAE luminosity function. We find 13 LAEs as compared to 29 foreground galaxies, in very good agreement with the modeled foreground counts predicted in Dressler et al. (2011a) that had been used to estimate a faint-end slope of $\alpha = -2.0$ for the LAE luminosity function. A 32% LAE fraction, LAE/(LAE+foreground), within the flux interval $F = 2 - 20 \times 10^{-18}$ ergs s⁻¹ cm⁻², constrains the faint end slope of the luminosity function to $-2.35 < \alpha < -1.95$ (1σ). We show how this steep LF should provide, to the limit of our observations, $M_{UV} \sim -16$, more than 20% of the flux necessary to maintain ionization at $z = 5.7$, with a factor-of-ten extrapolation in flux reaching more than 50%. This is in addition to a comparable contribution by brighter Lyman Break Galaxies $M_{UV} \lesssim -18$. We suggest that this bodes well for a sufficient supply of Lyman continuum photons by similar, low-mass star forming galaxies within the reionization epoch at $z \approx 7$, only 250 Myr earlier.

Subject headings: galaxies: high-redshift – galaxies: evolution – galaxies: formation

1. INTRODUCTION

Our understanding of galaxy evolution during the epoch of reionization has improved with the deep near-IR imaging from WFC3 on the Hubble Space Telescope. Numerous *Lyman-break* galaxies (hereafter, LBGs) have been found at redshifts $z = 6-9$, with a *luminosity function* (hereafter, LF) that spans a factor of ~ 100 in brightness (e.g., McLure et al. 2013; Ellis et al. 2013; Bouwens et al. 2014; Oesch et al. 2014). Although the photometric redshifts of these young

galaxies are reasonably secure, spectroscopic confirmation of Ly α emission has proven elusive in most cases (Fontana et al. 2010; Pentericci et al. 2011; Schenker et al. 2012; Caruana et al. 2012, 2014; Bunker et al. 2013). There is mounting evidence that this is due to a significant fraction of remaining HI that substantially attenuated any Ly α emission escaping these young objects (Stark et al. 2010; Ono et al. 2012; Treu et al. 2013; Tilvi et al. 2013; Momose et al. 2014; cf. Dijkstra et al. 2014).

Young stellar populations in early galaxies were the likely sources of high-energy ($E > 13.6$ eV) photons responsible for reionization of the intergalactic medium (IGM). However, it is well known that the brighter LBGs, $L \gtrsim L^*$, provide a small fraction of the required flux, so that much larger numbers of fainter, unobserved galaxies would be needed to balance or exceed the ionizing budget (Bunker et al. 2010). In fact, recent surveys that reach deeper do suggest that the LBG LF

*This paper includes data gathered with the 6.5 meter Magellan Telescopes located at Las Campanas Observatory, Chile.

Electronic address: dressler@obs.carnegiescience.edu

Electronic address: alaina.henry@nasa.gov

Electronic address: cmartin@physics.ucsb.edu

Electronic address: sawicki@ap.smu.ca

Electronic address: pmc2@obs.carnegiescience.edu

Electronic address: edwardv@obs.carnegiescience.edu

is steep, with faint-end slope $\alpha \sim -2.0$ (Bradley et al. 2012; Alavi et al. 2014; Schmidt et al. 2014; Bouwens et al. 2014). Though the *observed* LBGs account for $\sim 10\text{--}20\%$ of the required Lyman-continuum (LyC) flux, if a slope of $\alpha \sim -2.0$ continues to a luminosity $M_{UV} \sim -13$, then LBGs could account for all of the flux required for full reionization (Robertson and Ellis 2012; Robertson et al. 2013; Schmidt et al. 2014; Robertson et al. 2015).

Even with sufficient numbers, however, it is not certain that LBGs can supply sufficient LyC photons into the IGM: at redshifts $z = 5\text{--}6$, where neutral hydrogen is gone from the IGM, Ly α emission is only sometimes detected in LBGs (e.g., Shapley et al. 2003; Kornei et al. 2010; Stark et al. 2010; cf. Curtis-Lake et al. 2014). Therefore, it is important to investigate the contribution of LyC photons by the class of galaxies *defined* by strong Ly α — the *Ly α -emitters* (LAE). As described by Schaerer (2014), LAEs and LBGs at high redshift are closely related star forming systems whose differences in observable properties could be due entirely to differences in dust content. The lower (on-average) stellar mass of LAEs compared to LBGs may be connected to their systematically lower dust contents. It is possible, then, that the mature stellar populations in LBGs, evident in their strong stellar UV-continua, entrain enough dust to prevent many Ly α photons, and most LyC photons, from leaving the galaxy. For example, from observations comparing LBGs and LAEs at $z \sim 3$, Nestor et al. (2013) infer LyC escape fractions 2–4 times higher for LAEs. For this reason, the needed LyC photons may preferentially come from LAEs, where stellar continuum radiation is weak, and the dominance of emission is the signature of a younger starburst — perhaps the first major episode of star formation in the system.

The largest collections of LAEs at $z > 5$ come from narrow-band imaging surveys with the Subaru telescope (e.g., Shimasaku et al. 2006; Ouchi et al. 2008; Hu et al. 2010; Kashikawa et al. 2011). With the wide field-of-view of the SuprimeCam, narrow-band searches are an efficient way to find high redshift LAEs with luminosities $L \gtrsim L^*$, $\approx 10^{43}$ ergs s^{-1} . Thus, these studies have a good purchase on two of the Schechter function parameters, Φ^* and L^* , within their significant covariance. However, as explained in Dressler et al. (2011a), MNS2) and reiterated in §3.2 of this paper, detections of LAEs below L^* become rapidly incomplete for narrow-band observations of $\sim 150\text{Å}$ FWHM. Although some fainter objects are detected, incomplete sampling makes such data at $z = 5.7$ unsuitable for measuring the faint-end slope α .

Our *Multislit Narrowband Survey*, hereafter MNS, was specifically designed to produce complete samples of LAEs up to ten-times fainter than the narrow-band imaging surveys. Basically, this is accomplished by searching the same low-OH-background part of the spectrum as for imaging surveys for $z = 5.7$ LAEs (8110–8270Å), but by adding a grism or grating to disperse the light so that each emission-line-detection competes against a ten-times-lower sky background. The origin of the technique, and our application of it using the 27 arcmin-diameter field of the IMACS f/2 channel, is detailed in Martin et al. (2008, MNS1) and in MNS2.

MNS2 describes the analysis of an excellent observing run in 2008 that produced ~ 20 hours of integration for each of two fields, netting a sample of 210 single-emission-line-only sources that were candidate LAEs at $z = 5.7$. These spectra reached a 50% completeness at a line flux of $F = 3.5 \times 10^{-18}$ ergs s^{-1} cm^{-2} , sufficiently faint for the first credible measure-

ment of the faint-end-slope of the LAE luminosity function (hereafter, LF). However, because of the relatively low spectral resolution of $\approx 10\text{Å}$ FWHM and the $\sim 150\text{Å}$ coverage of the search spectra, LAEs could not be reliably separated from foreground galaxies producing [O II], [O III], H β , or H α emission, which together were expected to outnumber the LAEs by about 2-to-1. In MNS2 we used published results of counts of these foreground sources — extrapolated to the fainter limits of the MNS survey — to statistically correct for the foreground contamination and construct the residual LAE LF. This process depended most sensitively on the faint-end slope of each of the foreground populations, whose value and range we needed to estimate. Our best estimates of these quantities led to a faint-end slope of the LAE LF of $\alpha \approx -2.0$, but values as low as -1.5 or as high as -2.5 could not be ruled out.

Confirmation of a steep slope for LAEs at $z \sim 6$ has important implications for questions of galaxy formation, the production of heavy elements in the universe, and reionization, so we have been strongly motivated to confirm the result of a steep slope of the LAE LF forecast by our statistical correction for foreground contamination. Accomplishing this requires higher dispersion spectra for a statistically significant sample of the faintest LAE candidates. Our first efforts to do this have been described in Henry et al. (2012, MNS3), where LAEs were positively identified in the COSMOS field using spectra from Keck-DEIMOS with a resolution of $\lambda \approx 2\text{Å}$; these results are briefly reviewed in §4.1. In this paper we present similar spectra for a significantly larger sample of faint LAEs in our 15h field (LCRIS), leading to a determination $\alpha = -2.15 \pm 0.20$, in good agreement with the results of MNS2.

The paper is organized as follows: §2 describes the new data taken with IMACS on Magellan; §3 describes how these objects were matched to those found in the low-resolution search, and the criteria for separating LAEs from foreground galaxies; §4 explains how we used these data to constrain the faint-end slope of the LAE LF; §5 explores the implication of this now-confirmed steep slope of the LAE LF for reionization; and §6 gives our conclusions.

We adopt cosmological parameters of $\Omega_m = 0.30$, $\Omega_\Lambda = 0.7$, and $H_0 = 70$ km s^{-1} Mpc $^{-1}$ throughout.

2. THE DATA: HIGHER DISPERSION SPECTRA OF CANDIDATE LAES

The experimental technique of the 2008 MNS search was to use 100 parallel long slits crossing the full field of view of the IMACS f/2 camera, a circle of 27 arcmin diameter. The spacing was chosen to allocate about ~ 70 pixels in the dispersion direction per slit, which covered a “low-OH-emission” spectral band of $\lambda = 8115\text{--}8250\text{Å}$ at 2.0Å pix^{-1} . The 2008 MNS search used this setup, described in MNS2, to cover ~ 55 sq arcmin ($\sim 10\%$ of the full f/2 imaging field) in both the COSMOS field and the Las Campanas Redshift Survey field (Marzke et al. 1999). Slits 1.5 arcsec wide produced a spectral resolution of 14Å for objects that fill the slits, but for the typical size and profile of the discovered single-line sources, and the good seeing conditions of the search (< 0.6 arcsec FWHM) a 10Å FWHM resolution was typical. Still, at this resolution, spectra of LAEs are usually indistinguishable from single-emission-line foreground galaxies, since a resolution of less than $\lesssim 5\text{Å}$ is required to resolve the characteristic asymmetry of most Ly α emission lines, or to split the dou-

blet of [O II] foreground sources at $z \approx 1.2$. Because these data could not be used to unambiguously identify the LAEs at $z \approx 5.7$, the result from MNS2 of a steep slope of $\alpha \approx -2.0$ for the LAE LF depended on a statistical correction for the foreground contamination. Since this further depended on an extrapolation of the LFs for foreground sources to fainter limits than observed, the putative steep slope of MNS2 required further spectroscopy, to identify LAEs on an individual basis.

Such follow up spectral observations at 2-3 Å FWHM resolution were planned with both IMACS and Keck-DEIMOS starting in 2010. Observations planned in 2010, 2011, and 2012 for IMACS on Magellan-Baade were thwarted by poor weather, but observations in 2010 and 2011 with DEIMOS of LAE candidates in the COSMOS field were moderately successful in terms of observing conditions. The DEIMOS observations confirmed 6 LAEs from the faint sample; the basic results of MNS3 are reviewed in §4.1.

In April 2013 and March 2014, two mostly-clear 5-night runs at Las Campanas Observatory, with average, on-target seeing of 0.68 arcsec and 0.71 arcsec (approximately the median seeing at Magellan), were successfully completed using IMACS in f/4 mode (Dressler et al. 2011b) with a 600-l/mm +13° blaze grating, delivering a scale of 0.378 Å pix^{-1} and a spectral resolution (1.0 arcsec-wide slit) of $\sim 3 \text{ Å}$. The detector readout was rebinned by a factor-of-two in the spatial direction to increase signal over read noise, resulting in a scale of $0.22 \text{ arcsec pix}^{-1}$. A single slit mask was designed and fabricated for each year; each mask targeted LAE candidates in the 15h field of the *Las Campanas Redshift Survey* (Marzke et al. 1999). The position angle of slits was rotated by 90° from that of the long slits in the 2008 search mask, in order to place *along* the slit the coordinate that includes a degeneracy between sky position and line wavelength. The multi-slit masks of the IMACS f/4 cover a field of 15 arcmin x 15 arcmin. For the 2013 and 2014 runs, total integration times were 27.4 and 17.5 hours, respectively. The spectral range extended out to 9000 Å for all spectra, and for most extended down to $\sim 6000 \text{ Å}$, important for confirming those cases where H α was the line detected in the search window.

The new IMACS f/4 spectra were reduced using the *COSMOS* software package — <http://code.obs.carnegiescience.edu/cosmos/Cookbook.html>, augmented by programs written in Python by Kelson that facilitated the reduction of emission-line only sources, a departure from the common data reduction with *COSMOS* that makes use of object continua for fine-tuning object detection. Wavelength calibration and registration were performed using He+Ne+Ar lamp spectra taken in proximity to each set of science frames, while the modeling and subtraction of sky was done using the Kelson (2003) procedure. The reductions produced 2D frames of sky subtracted spectra that were shifted and added using *IRAF* ‘imcombine’ to produce a single frame for each year’s observations. These were examined with *Viewspectra*, a *COSMOS* routine for interactive examination of 2D spectra and for extracting 1D spectra.

Redshifts were measured for 45 of the 52 LAE candidates (“single-emission-line, no-blue-continuum sources” — see MNS2), an 87% success rate of recovering the targets from the 2008 search catalog. The other 13% failed to show an emission-line at or near the predicted spatial or wavelength position; in fact, none of these showed a convincing line over the full wavelength band. Twelve of the 52 candidates

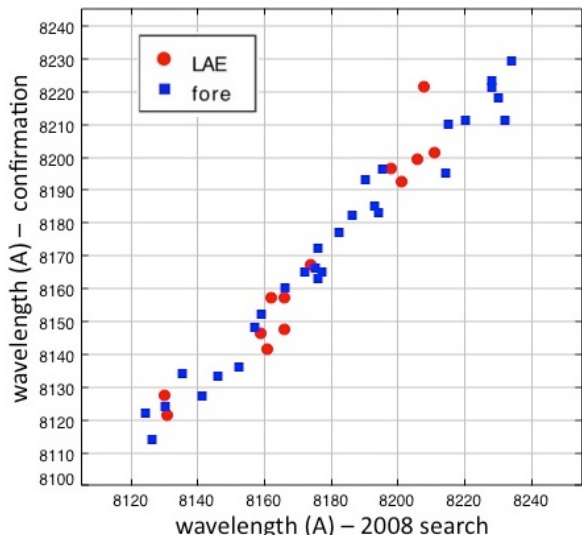


FIG. 1.— Wavelengths of single-emission-line sources from the 2008 search for faint LAEs compared to confirmation observations with higher spectral dispersion in 2013 and 2014. The dispersion of 5 Å and offset of 9 Å is dominated by uncertainties in the 2008 search data, for which wavelength calibration is difficult. The apparent clumping of the LAEs into three systems with a typical separation of $\sim 200 \text{ km s}^{-1}$ is likely to be real and indicative of a significant cosmic variance.

were repeated in the 2014 spectroscopy. Nine of the repeats were recovered spectra in good agreement with the 2013 data, while for three no object was found, as in 2013.

3. RESULTS

The final sample consists of 45 spectra: 13 sources are identified as LAEs and 32 as foreground galaxies (identified through criteria described below). For 3 of foreground galaxies the recovered emission line was an order-of-magnitude brighter than that of the 2008 candidate.¹ These were judged to be cases where the LAE candidate was actually an HII region of a foreground galaxy, and the galaxy to which it belonged revealed when the slit orientation was changed by 90° to remove the wavelength-position ambiguity (see §2). Also, two of the foreground galaxies are excluded from the following analysis because, though they *are* confirmations of the 2008 candidate data, they have fluxes of $F = 27 \text{ \& } 84 \times 10^{-17} \text{ ergs s}^{-1} \text{ cm}^{-2}$: this is a factor-of-ten brighter than the flux interval we are interested in. The probability of finding a LAE this bright is less than 1% for the area covered by our survey. This leaves a sample of 13 LAEs and 27 foreground galaxies covering the range in flux $F = 2\text{--}20 \times 10^{-18} \text{ ergs s}^{-1} \text{ cm}^{-2}$, the relevant range for the determination of the faint-end slope of the luminosity function (fainter than L^*), as can be seen in Figures 10 and 11 of MNS2.

Concerning the measured fluxes of these sources, we note that photometry is problematical with spectroscopic data, due to the uncertainty of object position with respect to slit and the fact that some objects are bigger than the slit width (slit losses). For the faint objects of our study, sky subtraction and flat-fielding errors add to the difficulty. Furthermore, the detections at the flux limit of our sample, $F \sim 3 \times 10^{-18} \text{ ergs s}^{-1} \text{ cm}^{-2}$, have only signal-to-noise ratio (hereinafter, SNR) $\approx 3\text{--}5$ (see MNS2, Figure 3). The combined

¹ One of these was at the wrong spatial position and another had a strong continuum as well.

effect, evident in comparing our 2008, 2013, and 2014 data sets, is that photometry accurate to $\lesssim 10\%$ is not possible — typical errors are typically two or three times larger. In MNS3 we implemented a maximum-likelihood methodology capable of deriving the luminosity function in the presence of such photometric scatter and the uncertain positions of objects within the slits of the blind search. In this paper we take an alternative approach based on the LAE fraction which, as we show in §4, is also robust to these effects.

We retained the fluxes measured from the 2008 search spectra for the following analysis, however, among the 27 foreground sources of the final sample (but for none of the LAE sample) 4 objects were significantly brighter in the 2013, 2014 spectroscopy than in the discovery spectra, 2 by $\sim 30\%$ and 2 by a full factor-of-two. We judged these to be cases of slit-losses in the discovery spectra — a reasonable fraction — and revised them to the higher value.

3.1. Criteria for discriminating $z = 5.7$ LAEs from foreground galaxies

We have a high degree of confidence in the sample of LAEs we report here. The criteria that underlie this confidence is a series of qualifications. To be considered a "recovered candidate" from the the 2008 search, an emission line in the 2013 and/or 2014 spectra must agree with the wavelength found in the search data. Figure 1 shows this comparison for both the LAEs and foreground sources in the new data. Compared to the $\sim 135 \text{ \AA}$ range of the bandpass, the $\sim 5 \text{ \AA}$ scatter in the relation is small, ergo, there is no question that the recovered objects are the ones found in the 2008 search.² The recovered spectra were also required to lie within ± 2 arcsec of the spatial position on the slit predicted from the 2008 search data.

Further criteria for identifying $\text{Ly}\alpha$ emission come from the spectra, most of which are shown in Figures 2 and 5. In Figure 2, the extracted spectra have been smoothed by gaussian of width $\sigma = 1.0 \text{ \AA}$ (compared to the instrumental resolution of $\sim 2.5 \text{ \AA}$) and plotted centered on the line detection, over an interval of 60 \AA . In Figure 5, in the Appendix, we show the left and middle panels of the Figure 2 spectra over the full 135 \AA bandpass and essentially unsmoothed, to allow a better judgement of the prominence of the detected lines and the noise background. Figure 5 also records the SNR for each of the detected lines, demonstrating that the features are all detected at $\text{SNR} > 6\sigma$.

The second criterion comes from the clear identification of foreground objects from their spectra. $[\text{O II}]$ emission at $z \approx 1.20$ accounts for $\sim 60\%$ foreground contamination. As shown in the middle panel of Figures 2 (and even more clearly in Figure 5), the $[\text{O II}]$ doublet ($\lambda\lambda 3726, 3729 \text{ \AA}$) is well-resolved and each line easily distinguished, even for the faintest objects. Emission-line galaxies at $z \approx 0.64$ are also a major component of the foreground: the $\lambda 5007$ line of $[\text{O III}]$ is shown for 5 out of the 8 cases (right-hand column of Figure

2) and in all these cases $\lambda 4959$ is also detected, and usually $\text{H}\beta$ as well. $\text{H}\alpha$ at $z = 0.25$ and $\text{H}\beta$ at $z \approx 0.68$ accounts for only 10% of the foreground, and only one of these show accompanying $[\text{N II}]$ emission, but in all but one case $\text{H}\alpha$ is ruled in or out by the detection of $[\text{O III}]$ at an observer-frame wavelength of $\sim 6250 \text{ \AA}$. A comparatively rare $[\text{Ne III}]$ line, confirmed by the presence of $[\text{O II}]$, was also found, but together $[\text{O II}]$, $[\text{O III}]/\text{H}\beta$, and $\text{H}\alpha$ should account for 99% of the foreground, since these are much stronger than any other lines from $[\text{O II}]$ to $\text{H}\alpha$. $\text{H}\gamma$ or $\text{H}\delta$ emission could have been found, but $[\text{O II}]$ would always accompany them.

The remaining 13 emission lines, shown in the left column of Figure 2, are identified as $\text{Ly}\alpha$. Although their principal criterion is through elimination of other possibilities, there is additional verification from the typically $10\text{--}20 \text{ \AA}$ width of $\text{Ly}\alpha$ emission. The characteristic asymmetry of $\text{Ly}\alpha$ is seen in 8 of the 13 objects, and 3 others, although not clearly asymmetric at this SNR are clearly too broad to be foreground lines. In addition, $[\text{O III}]/\text{H}\beta$, $\text{H}\alpha$ are all ruled out — as described above, and the small velocity broadening expected for these foreground dwarf galaxies ($M \sim -17$), $\sigma \lesssim 50 \text{ km s}^{-1}$, rules out the possibility of broadened $[\text{O II}]$. Three additional $\text{Ly}\alpha$ lines appear to be narrower, although only one appears as narrow as the $\sim 2.5 \text{ \AA}$ instrumental resolution. These resemble some of the fainter LAEs from the Subaru-SuprimeCam studies (Kashikawa et al. 2011) and two examples from our own Keck-Deimos spectra (MNS3). For the three found here (labeled 1.9, 2.6, and 3.5 in Figure 2), we rule out $[\text{O II}]$, $[\text{O III}]/\text{H}\beta$, and $\text{H}\alpha$ (by lack of $[\text{O III}]$ emission — see above) as alternative identifications.

In summary, we consider these 13 $\text{Ly}\alpha$ identifications to be secure, and the foreground identifications as well.

Basic data for each of these 13 LAEs, including position and SNR of detection, are given in Table 1.

3.2. These are the faintest LAEs yet detected at $z \sim 6$

All 13 LAEs are fainter by a factor of 2 to 5 than the completeness limits of two Subaru Suprime-Cam narrow-band surveys, COSMOS $F \approx 2 \times 10^{-17} \text{ ergs s}^{-1} \text{ cm}^{-2}$, and the Subaru Deep Field, $F \approx 1.6 \times 10^{-17} \text{ ergs s}^{-1} \text{ cm}^{-2}$ (see Figure 1 of Takahashi et al. 2007). Although Kashikawa et al. (2011) include LAEs 2-3 times fainter than these limits, the detections have large errors, $\text{SNR} < 3$, with the result that they are drawn from a very incomplete sample. For this reason, the faint-end slope of the LAE LF is unconstrained by the Subaru narrow-band data, as is apparent from the renderings of the LF in Kashikawa et al.'s Figures 7 & 9. Our MNS study has the only sample of LAEs that constrains the faint end slope of the LAE LF at $z = 5.7$.

The flux level reached in this study is comparable to that achieved by Rauch et al. (2008) in their study of $\text{Ly}\alpha$ -emitters at $2.6 < z < 3.7$, from a heroic 92-hour integration with VLT FORS2.

By accessing the faintest LAEs yet detected at $z \sim 6$ we are detecting galaxies that have been previously only included in the ionization budget by extrapolation. Although none of the 13 LAEs discussed here show a clear continuum flux redward of $\text{Ly}\alpha$, our spectroscopy provides a weaker limit than deep imaging. MNS3 made simulations, based on the $z \sim 6$ UV continuum LF (Bouwens et al. 2007) and the Stark et al. (2011) equivalent width distribution, to estimate that the LAEs in our survey should have $M_{\text{UV}} \approx -16$ to -17 and thus be undetected at the depth of HST *Ultra Deep Field*. There-

² The dispersion in wavelength, as well as the $\sim 10 \text{ \AA}$ shift between the search data and the follow-up data is dominated by the former. Repeat measurements in 2014 of 12 objects observed in 2013 show a typical error of less than 1 \AA , from well-calibrated arc lines spanning of several thousand angstroms. There are no comparison arc lines in the narrow band of the 2008 search data, which covers only $\lesssim 150 \text{ \AA}$. We used the narrow-band interval itself to define the wavelength scale, but the bandpass shifts with angle from the optical axis, and the "venetian blind" mask made used in the LCRIS (15h) search added additional uncertainty because of departure from sphericity of the highly perforated mask, another source of error in the wavelength.

fore, our LAE sample is an extrapolation of the faintest LBGs beyond their limit $M_{UV} \sim -18$. The *lensed* galaxies from the HST *Frontier Fields* are expected to reach LBGs at the depth of the present sample for LAEs. To detect Ly α in that deeper LBG sample with the technique used here will probably require the new generation of 30-m telescopes, although deep HST-WFC3 grism observations might confirm LAEs at this even fainter limit.

4. MEASURING THE SLOPE OF THE LAE LUMINOSITY FUNCTION

The slope of the LAE LF is the critical determinant of the contribution of low-luminosity LAEs to reionizing flux in the early universe. Uncertainties in the other Schechter function parameters — a lower characteristic luminosity L^* or even a lower space density Φ^* — are quickly overcome if the slope is steep, $\alpha < -1.5$, needing only a factor-of-two more "depth" to reach the photon flux capable of reionizing the universe.

In MNS2 we presented a sample of 210 galaxy spectra that showed only a single emission line in a 140 Å-wide search band centered at $\lambda \approx 8180$ Å. The source counts of these candidate LAEs rose rapidly with decreasing flux, but we recognized that most of these sources had to be foreground galaxies. Lacking the high-resolution spectra we now have (or any reliably way separate LAEs from foreground), we used published data from Taniguchi et al. (2007) of foreground [O II], [O III], and H α emitters to remove the foreground statistically, leaving a possible LAE LF. In particular, subtracting our best Schechter-function fits to the foreground counts (shown in Figure 8 of MNS2) produced an LAE LF with a faint end slope $\alpha \approx -2.0$ that matched up well with an LAE LF with the same slope from Shimasaku et al. 2006 (see MNS2, Figure 10) — one of three acceptable fits to the LAE LF they made using their sample of $L \gtrsim L^*$ LAEs.

Unfortunately, the LAE LF we derived with this method was not unique: our Schechter fits to the LFs of the 3 foreground populations could not be tightly constrained because they required an extrapolation to the faint flux levels of our study: the Taniguchi et al. data come from narrow-band imaging observations that, like the LAEs, become rapidly incomplete for $\log F < -17.0$. For this reason, we needed to consider perturbations on the "best-fitting" foreground LFs to assess the robustness of our result of an LAE LF with slope $\alpha \approx -2.0$.

In that exercise, we learned that we could not rule out a much shallower slope for the LAE LF, even to $\alpha = -1.0$, or even a slope as steep as $\alpha = -2.5$. Here we use the term "realization" to refer to each of the possible LAE LFs we generate by modifying the foreground LFs within their uncertainties. In the process of making such realizations in MNS2, we also found — not surprisingly — that the fraction of LAEs, $\text{LAE}/(\text{LAE}+\text{foreground})$ was a sensitive function of the LAE LF slope. The power of the new data presented in this paper is that even a small sample of 40 LAE+foreground sources can greatly reduce the range of acceptable realizations. This is the approach that we now describe.

In MNS2 we adopted the Shimasaku et al. Schechter LF fits to their LAE data³ with faint end slopes of -1.0, -1.5, and -2.0, as models for the different "realizations" of the LAE LF we had made by subtracting slightly different levels of foreground contamination. This means that each realization was made to match a Shimasaku et al. LF of slope α , including

its L^* and Φ^* 'normalization.' The Shimasaku et al. LFs predict 16-18 bright LAEs ($\log F > -17.0$) — depending on the slope — over the volume of our survey (see MNS2 Figure 10). A deficiency of that analysis, however, was the graphical, rather than analytical, comparison of our realizations of the LAE LF with the Shimasaku et al. models (MNS2 Figure 11). We rectify this here by measuring the steepness of the cumulative LAE LF in the Shimasaku et al. models, $R = N_{\text{LAE}}(\log F > -17.6)/N_{\text{LAE}}(\log F > -17.3)$ — the ratio of the integrated LAE counts over this flux interval, and adjusting the foreground LF fits (within their uncertainties) to achieve the same quantity for each LAE LF realization.⁴ (Each realization also matches the Φ^* normalization discussed above.) Table 2 lists the R values for each model and realization and the values of α , $\log L^*$, and $\log \Phi^*$ for [O II], [O III], and H α foregrounds that were used to achieve the match.⁵

If we now calculate $\text{LAE}/(\text{LAE}+\text{foreground})$ — the LAE fraction — over the interval $F = 2 - 20 \times 10^{-18}$ ergs s⁻¹ cm⁻², for each of these three realizations, we find values of 0.099, 0.142, and 0.260, corresponding to expected number of LAEs of approximately 4, 6, and 10, respectively, for a 40-object sample. These are to be compared with the 13 we actually found. In the next section we describe a simple test of the likelihood of these and other realizations that, in the end, constrain the allowable realizations to a small range of slopes.

4.1. The LAE fraction of different realizations and comparison with observations

In §3 we discussed the substantial uncertainties in the fluxes of our faint sources. Even at this level of accuracy, the data are probably good enough to fit a Schechter function — as we did in MNS3, but in this paper we use a new method that is robust to photometric errors, measuring only the LAE fraction $\text{LAE}/(\text{LAE}+\text{foreground})$ over a flux interval, $F = 2 - 20 \times 10^{-18}$ ergs s⁻¹ cm⁻², and comparing this with expectations based on luminosity functions of varying slopes. This ratio is well measured — despite the uncertainty in fluxes — because both LAEs and foreground galaxies are well bounded, on the faint end by the flux limit of all detections, and on the bright end by L^* for both LAEs and foreground. Figure 3 shows that for $F > 2 \times 10^{-17}$ ergs s⁻¹ cm⁻² there is only one foreground galaxy out of the total sample of 27, and no LAEs.

Table 3 lists realizations of the MNS2 data we made for the 3 Shimasaku et al. models but also spanning the full range of plausible faint-end slopes, $-1.5 > \alpha > -2.5$, in steps of 0.1. These interpolated Shimasaku et al. models were generated by quadratic fits to $\log L^*$ and $\log \Phi^*$ and, each as a function of α , based on the three models of slope $\alpha = -1.0, -1.5$, and -2.0 . Table 3 lists these Schechter function parameters

⁴ R is a proxy for the asymptotic slope α , which our data — although well below L^* — do not reach.

⁵ Although cosmic variance of order $\sim 30\%$ in the Φ^* normalizations of foreground LFs are expected in fields this size, we made changes of only Φ^* of only $\leq 10\%$ from the LFs we adopted from Taniguchi et al. (2007). Beyond this, non-physical LFs result, that is, LFs with negative LAEs or diverging with increasing depth. Cosmic variance is not an issue in this study because the foreground LFs had already been measured in one of our fields, COSMOS, and the LCRIS and COSMOS fields have similar distributions of number counts versus flux (compare Figures 1 and 2 in MNS2), and also consistent with the actual measurement of foreground contamination we present here. We note, however, that the method we describe here would work for another field of this size with significantly different levels of the foregrounds, and would produce a $z = 5.7$ LAE LF with its appropriate cosmic variance of $\sim 20\%$ for fields of this size.

³ Parameters for these LFs are closely matched by the Hu et al. 2010 study.

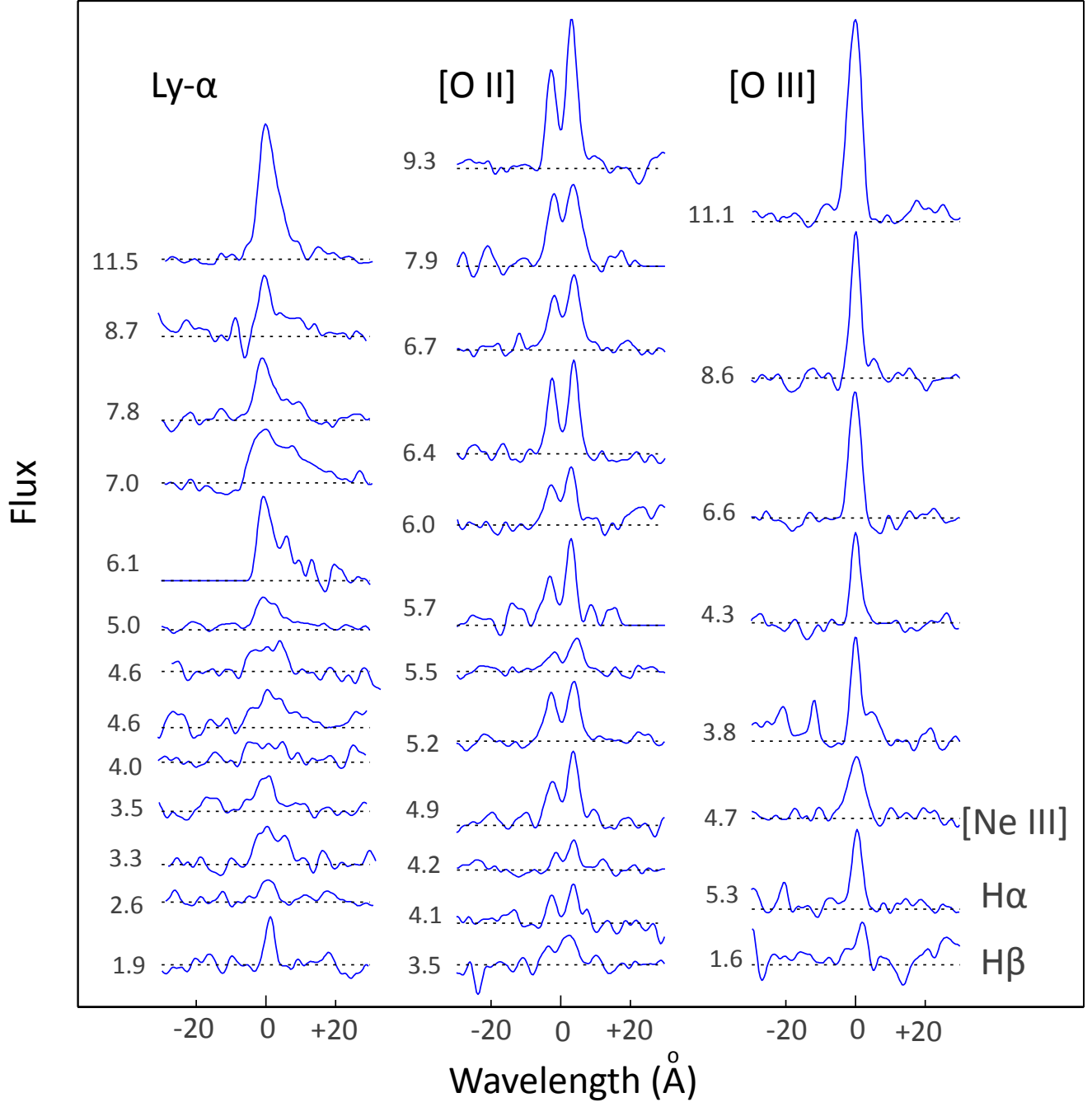


FIG. 2.— Spectra of LAE candidates from 2013 and 2014 observations with IMACS on Magellan-Baade. The number to the left of each spectrum is its flux in units of $10^{-18} \text{ ergs s}^{-1} \text{ cm}^{-2}$. The left column shows the 13 detected LAEs at $z \approx 5.7$. The middle column shows 12 of the 16 detected [O II] emitters at $z \approx 1.20$, which account for $\sim 60\%$ of the foreground sample. The four [O II] detections not shown are strong signals with fluxes of 6.7, 8.1, 10.7, and 13.2, omitted for clearer presentation of the remaining spectra.) The third column shows 8 of the remaining 11 foreground spectra, 5 of the 8 detected [O III] emitters ($z \approx 0.64$, $\sim 30\%$ of the foreground) and the three remaining foreground sources, H α , H β , and [Ne III].

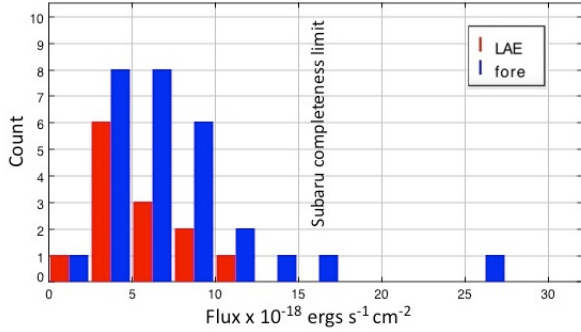


FIG. 3.— Flux distribution for LAE and foreground sources, showing the increasing fraction of LAE compared to the foreground population with decreasing flux.

for each model and its R value, which is compared to the R value of the realization of the data that matches this model. For a sense of how much the foregrounds need to be adjusted to produce this full set of models we also include the α , $\log L^*$, and $\log \Phi^*$ values for the [O II] and [O III] LFs, which account for 90% of the foreground. The progression of these values from $\alpha = -1.0$ to -2.5 show that, while these values are not “unique,” there is a predictable manipulation of the parameters that generate the full range of realizations.

With this full range of realizations of the 2008 data, each matching a Shimasaku et al. LAE LF, we use our new data to test the likelihood of each. This was done by calculating the predicted LAE fraction, $\text{LAE}/(\text{LAE}+\text{foreground})$, over the range $F = 2 - 20 \times 10^{-18} \text{ ergs s}^{-1} \text{ cm}^{-2}$ for each realization, and comparing it to the LAE fraction of our new data, 13/40, or 0.325.

We use a Monte Carlo test to determine how often the *observed* LAE fraction of 0.325 would be reproduced in each of our realizations of the LAE LF — these results are shown in Table 3. For example, the LAE LF realization with $\alpha_{\text{LAE}} = -1.0$ has an LAE fraction of 0.099 — 4 LAEs out of 40 total (single-emission-line-only) detections for this nearly flat slope. The Monte Carlo test uses a random draw from a 40 object sample to determine that the observed number of 13 LAEs would be found only once in 10,000 trials if only 4 are expected. This possible LAE LF is therefore ruled out. The slopes -1.5 and -2.0 , considered in MNS2, have LAE fractions of 0.142 (~ 6 LAEs) and 0.260 (~ 10 LAEs), corresponding to probabilities of 0.19% and 22%, of finding 13 LAEs. The “best fit” of $\sim 40\%$ is between the LAE LF realizations of $\alpha = -2.1$ and -2.2 . The likelihood falls for greater slopes: for the realization $\alpha = -2.5$ the LAE fraction is 0.477 (~ 19 LAEs) and the probability of finding *as few* as 13 LAEs for a 40 object sample has decreased to $(100-98) = 2\%$. In comparison with MNS2, the flat and modest slopes of -1.0 and -1.5 for the LAE LF — although compatible with the brighter data of Shimasaku et al. — produce too few LAEs and are ruled out by our 13 LAE detections, as is the -2.5 slope, which produces too many.

The result is a probability distribution that is close to Gaussian, with the mean value of $\alpha = -2.15$ and a standard deviation of 0.20. The 2σ value is reached at -1.75 , as expected, but the 2σ on the steep side comes in at -2.50 rather than -2.55 . The shot noise associated with this relatively small sample suggests a systematic error of ~ 0.1 in the slope.

The LAE LF with a faint-end slope of $\alpha = -2.15$ passes two other tests that show how well it fits the data. The first considers how well the percentage of *each* foreground population

in our new data compares to values derived in MNS2 for the COSMOS field (where there are data for the foregrounds, as described in MNS2), but applied to both of the 2008 search fields. (In this paper we used that 2008 model as a starting point to set the Φ^* of each foreground.) With our best-fitting realization of slope, $\alpha = -2.15$, the relative foreground contributions over the $\log F = -16.8$ to -17.7 range are: 57% for [O II] compared to observed 63% (1σ bounds 42% - 70%); 34% [O III] compared to observed 30% (23%-45%); and 9% for H α compared to observed 7% (4% to 16%). This validates the foreground model used to derive slopes for the LAE LF of $\alpha \sim -2.0$ in MNS2, that is, the parameters for the Schechter functions describe the foregrounds well.

The second test concerns the LAE-to-foreground ratio as a function of decreasing flux. Although we have simply gathered together all the LAEs and foreground galaxies in the flux interval and focused on a single parameter — the LAE fraction, we can learn something from Figure 3 about the distribution — the increasing fraction of LAE/foreground with decreasing flux. Again, the best fit LAE LF derived with the new data is in agreement this observed trend: brighter than $\log F = -17.0$, foreground galaxies in the model outnumber LAEs by 9 to 1. At $\log F = -17.0$ this ratio has dropped to 4.4 to 1, and at $\log F = -17.6 \text{ ergs s}^{-1} \text{ cm}^{-2}$ LAEs are almost one-to-one with the foreground. For all the uncertainty in the fluxes, this is what the data of Figure 3 show.

4.2. Comparison with the Keck-DEIMOS results

In MNS3 the results of Keck-Deimos observations in 2011 and 2012 were presented and analyzed, including the first recovery of faint LAEs in MNS, 6 LAEs with fluxes between $F = 5 - 10 \times 10^{-18} \text{ ergs s}^{-1} \text{ cm}^{-2}$. A maximum likelihood technique was used to find a LF faint-end slope of $\alpha \sim -1.7$, shallower than found here, but the $\alpha \approx -2.0$ slope found in MNS2 using a statistical correction of the foreground contamination is within the 1σ uncertainty of the both MNS3 and the present result. The methodology used here to measure the faint-end slope is not easily applied to the MNS3 data, since there was a prioritization of DEIMOS targets — based on previous low-resolution IMACS spectroscopy — that favored objects that were narrowed-down to be either LAE or [O II] foreground over those without additional information following the original detection in the 2008 search data (see MNS3). Also, the LAEs found in MNS3 cover only the brighter part of this paper’s sample (see Figure 3), which means that the LAE fraction is expected to be smaller, 26% instead of 33% — according to the best-fit model we find here. Still, it appears that the result of MNS3 points to a flatter slope. We stress, however, that the derivation of a probable $\alpha = -2.15$ slope in this study is completely compatible with the data and analysis of MNS3.

A strength of the present work is that the LAE and foreground spectra represent a nearly complete ($\sim 85\%$ of targeted objects) sample, randomly selected by the spatial constraints of the multislit mask technique, that should be unbiased. This simplifies the analysis here. The unbiased selection of targets, and the much larger sample of confirmed LAEs, makes the present work the best assessment of the faint LAE population to-date, providing the strongest constraint on the faint-end slope α of the LAE LF.

5. THE LAE POPULATION PROVIDES A SUBSTANTIAL FRACTION OF REIONIZING PHOTONS

At $z = 5.7$, our sample lies past the redshift of full reionization at $z = 6.0$ — our LAEs contribute to *maintaining* ioniza-

tion by balancing recombination. However, because $z = 5.7$ and $z = 6.0$ are separated by only by 64 million years, and by an additional 200 Myr to $z = 7$, it is reasonable to believe that our sample is representative of the similar emission-line galaxies *within* the reionization epoch. Furthermore, since HI absorption seems to substantially attenuate the Ly α signal at $z \gtrsim 7$ (see §1), observing LAEs at $z = 5.7$ may turn out to be the best epoch to study the properties of LAEs at earlier times.

In MNS2 we reviewed a number of issues that were related to the possibility that the faint-end slope of the LAE LF is steep, $\alpha \approx -2.0$, something that the present study confirms. The identification of these faint LAEs as systems of halo mass $10^{10} - 10^{11} M_{\odot}$, at a space density equivalent to several objects per today's L^* galaxy, motivated our contention that these are the likely progenitor components of L^* galaxies, and that these lower mass systems are the probable source of the metal enrichment of the IGM at this early epoch. In this connection, the resolved profiles of most of the Ly α sources presented in this paper have rest frame widths of several hundreds of kilometers per second, a necessary though not sufficient condition for ascribing a large outflow velocity, which additionally requires an as-yet-unmeasured local-standard-of-rest.

Here we consider only the ramifications of this now well-measured faint-end slope of the LAE LF at $z = 5.7$ for the question of the sources of reionization of the IGM. In a recent study motivated in part by the results presented here, Gronke et al. (2015) predict a Schechter-like slope of the LAE LF based on a model that uses the UV-LF of LBGs and the distribution of their Ly α strengths as a function of UV-luminosity and redshift (see also Garel et al. 2015). Gronke et al. predict a faint-end slope of $\alpha < -2.0$ for the LAE LF at $z > 4$ — somewhat steeper than the LF for LBGs galaxies — and that this slope holds until a turnover around $10^{40} \text{ ergs s}^{-1} < L < 10^{41} \text{ ergs s}^{-1}$. These predictions of a steep slope of the LAE LF in agreement with the measurement reported here, and its continuation to $L < 10^{41} \text{ ergs s}^{-1}$, bodes well for our argument that LAEs play a significant, perhaps even a dominant role in the reionization of the early universe, as we now show.

In MNS1 and MNS2 we derived the star formation rate (SFR) density required to maintain ionization at $z \sim 5.7$ from the LAE LF flux. The uncertain parameters for calculating this quantity are the production rate and escape fraction of Ly α and LyC photons and the clumping factor of the IGM. MNS1 derived the equation for the critical luminosity density \mathcal{L} in Ly α required to maintain ionization at $z = 5.7$,

$$(1) \quad \mathcal{L} = 3.0 \times 10^{-40} \text{ ergs s}^{-1} \text{ Mpc}^{-3} \times \zeta \times \left(\frac{1+z}{6.7} \right)^3 \left(\frac{\Omega_b h_{70}^2}{0.047} \right)^2$$

where

$$(2) \quad \zeta = C_6 (1 - 0.1 f_{\text{LyC},0.1}) \left(\frac{f_{\text{Ly}\alpha,0.5}}{f_{\text{LyC},0.1}} \right)$$

combines the clumping factor, the Ly α escape fraction, and the LyC escape fraction, normalized to values of 6, 0.5, and 0.1, respectively. A value of $\zeta \approx 1$ represents current estimates of these values.

The rising LF for faint LAEs we have confirmed here is an important step towards showing that galaxies at $z = 5.7$ are capable of maintaining ionization and, by implication, that a similar population of low-mass, low dust galaxies made a substantial contribution to reionization at $z \gtrsim 7$, only ~ 300 Myr earlier. As discussed in §3.2, the faintest LAEs in our

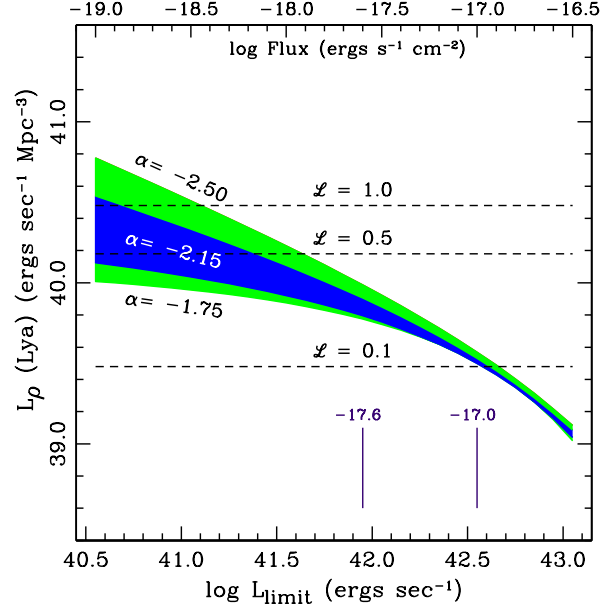


FIG. 4.— Level of luminosity density required for maintaining reionization at $z \approx 5.7$ with a population of faint LAEs. The blue and green shadings show the $\pm 1\sigma$ and $\pm 2\sigma$ bounds of a best-fit slope is $\alpha = -2.15$ and $\sigma = 0.20$. Within these limits, there is substantial progress toward reaching critical flux density, $\zeta = 1$: 22% is reached at the flux limit of our observations, 35% if the LF continues to a factor-of-three-fainter flux limit, and $\sim 56\%$ if it continues a full factor-of-ten. If the LyC escape fraction reaches as high as 20%, the full reionizing budget could be reached at that point. Such a higher escape fraction is consistent with trends of increasing redshift and decreasing luminosity found in lower-redshift samples, increasing the likelihood that LAEs alone can provide the critical flux density to complete reionization at $z \sim 6$.

sample are likely to have $M_{UV} \approx -16$ to -17 , thus they add to the fraction of reionizing flux found for the LBG population, whose limit is presently $M_{UV} \sim -18$.

In Figure 4 we reframe Figure 12 of MNS2 with the new limits on the faint-end slope, confirming that such systems played a substantial role in the ionization of the IGM. Figure 4 shows the luminosity-density in Ly α as a function of the limiting luminosity of the LAE LF that has been measured. The critical flux density, \mathcal{L} , from Eqn. (1), is shown for 10%, 50%, and 100% of the flux required for full ionization. The blue shaded region shows how 1σ limits on the faint-end slope map onto the reionization flux. Assuming a modest factor-of-three extrapolation in limiting luminosity of our faint-end slope, our observations already reach a level of $\sim 35\%$ of the critical density, and a factor of three further extrapolation brings us to the $\sim 55\%$ level.

A faint end slope $\alpha > -2.0$ is unphysical, of course, in the sense that extrapolation of this LF indefinitely is unbounded. However, there is no reason to suspect that the physics responsible for the steep interval found here — significantly steeper than for any lower-redshift sample of galaxies, continues to apply. A shallowing of the slope α or even a cutoff for much fainter LAEs would not be unexpected. Furthermore, the steep slope we find for the LAE LF may not be entirely due to a steep increase in the actual number of objects, since an increasing Ly α escape-fraction, also not unexpected in lower-luminosity (lower-mass) systems (Schaerer et al. 2011), could be partly responsible. Finally, we note that Figure 4 uses an escape fraction of LyC photons of only 10%, a conservative value that may also increase with higher redshift and lower-mass systems (Hayes et al. 2011; Blanc et al. 2011; Nestor et al. 2011, 2013; Dijkstra & Jeeson-Daniel 2013; Jones et al.

2012; Jones et al. 2013; Cassata et al. 2014). If so, reaching the full flux needed to maintain or drive reionization may be achieved with a continuation of the steep LF for only a factor-of-ten beyond the luminosity range covered in this study.

Finally, we note a recent study by Topping and Shull (2015) that suggests a boost in production efficiency — LyC photons per unit SFR — based on new models of rotating hot stars (see also Leitherer et al. 2014). Although we have used previous estimates of LyC production efficiency to facilitate comparisons with previous work, such changes would push the contribution of LAEs to reionization that much closer to, or above, the critical SFR density.

6. CONCLUSION

We have confirmed a steep faint-end slope of the luminosity function of Lyman- α emitters at $z = 5.7$ by finding a $\sim 32\%$ fraction of LAEs in a sample of 42 extremely faint emission-

line galaxies. A robust test shows that this fraction of LAEs is inconsistent with faint-end slopes much flatter than $\alpha = -1.90$, and that a slope of $\alpha = -2.0$ or greater has a high probability. A slope this steep suggests a substantial, perhaps dominant contribution by LAEs to maintaining reionization at this epoch, with a moderate extension of the $\alpha \approx -2.0$ slope by a factor of ~ 10 or to fainter systems needed account for much or even all the required flux. Considering the proximity in time of these LAEs to objects within the reionization epoch, it is reasonable to imagine that similar emission-line galaxies at $z > 7$ make a substantial contribution to reionization in the early universe.

7. ACKNOWLEDGMENTS

AH is supported by an appointment to the NASA Postdoctoral Program at the Goddard Space Flight Center, administered by Oak Ridge Associated Universities through a contract with NASA.

REFERENCES

- Alavi, A., Siana, B., Richard, J., et al. 2014, *ApJ*, 780, 143
 Blanc, G. A., Adams, J. J., Gebhardt, K., et al. 2011, *ApJ*, 736, 31
 Bouwens, R. J., Illingworth, G. D., Franx, M., & Ford, H. 2007, *ApJ*, 670, 928
 Bouwens, R. J., Illingworth, G. D., Oesch, P. A., et al. 2014, *arXiv:1403.4295*
 Bradley, L. D., Trenti, M., Oesch, P. A., et al. 2012, *ApJ*, 760, 108
 Bunker, A. J., Wilkins, S., Ellis, R. S., et al. 2010, *MNRAS*, 409, 855
 Bunker, A. J., Caruana, J., Wilkins, S. M., et al. 2013, *MNRAS*, 430, 3314
 Caruana, J., Bunker, A. J., Wilkins, S. M., et al. 2012, *MNRAS*, 427, 3055
 Caruana, J., Bunker, A. J., Wilkins, S. M., et al. 2014, *MNRAS*, 443, 2831
 Cassata, P., Tasca, L. A. M., Le Fevre, O., et al. 2014, *arXiv:1403.3693*
 Curtis-Lake, E., McLure, R. J., Pearce, H. J., et al. 2012, *MNRAS*, 422, 1425
 Dijkstra, M., & Jeason-Daniel, A. 2013, *MNRAS*, 435, 3333
 Dijkstra, M., Wyithe, S., Haiman, Z., Mesinger, A., & Pentericci, L. 2014, *MNRAS*, 440, 3309
 Dressler, A., Martin, C. L., Henry, A., Sawicki, M., & McCarthy, P. 2011a, *ApJ*, 740, 71, *MNS2*
 Dressler, A., et al. 2011b, *PASP*, 123, 288
 Dunlop, J. S., Rogers, A. B., McLure, R. J., et al. 2013, *MNRAS*, 432, 3520
 Ellis, R. S., McLure, R. J., Dunlop, J. S., et al. 2013, *ApJ*, 763, L7
 Fontana, A., Vanzella, E., Pentericci, L., et al. 2010, *ApJ*, 725, L205
 Garel, T., Blaizot, J., Guidoroni, B., et al. 2015, *arXiv:1503.06635*
 Gronke, M., Dijkstra, M., Trenti, M., & Wyithe, S. 2015, *arXiv:1502.00022*
 Hayes, M., Schaerer, D., Östlin, G., et al. 2011, *ApJ*, 730, 8
 Henry, A. L., Martin, C. L., Dressler, A., Sawicki, M., & McCarthy, P. 2012, *ApJ*, 744, 149, *MNS3*
 Hu, E. M., Cowie, L. L., Barger, A. J., et al. 2010, *ApJ*, 725, 394
 Jones, T. A., Ellis, R. S., Schenker, M. A., & Stark, D. P. 2013, *ApJ*, 779, 52
 Jones, T., Stark, D. P., & Ellis, R. S. 2012, *ApJ*, 751, 51
 Kashikawa, N., et al. 2011, *ApJ*, 734, 119
 Kelson, D. D. 2003, *PASP*, 115, 688
 Kornei, K. A., Shapley, A. E., Erb, D. K., et al. 2010, *ApJ*, 711, 693
 Leitherer, C., Ekström, S., Meynet, G., et al. 2014, *ApJS*, 212, 14
 Martin, C. L., Sawicki, M., Dressler, A., & McCarthy, P. 2008, *ApJ*, 679, 942, *MNS1*
 Marzke, R. O., Geller, M. J., Huchra, J. P., & Corwin, H. G., Jr. 1994, *AJ*, 108, 437
 McLure, R. J., Dunlop, J. S., Bowler, R. A. A., et al. 2013, *MNRAS*, 432, 2696
 Momose, R., Ouchi, M., Nakajima, K., et al. 2014, *MNRAS*, 442, 110
 Nestor, D. B., Shapley, A. E., Kornei, K. A., Steidel, C. C., & Siana, B. 2013, *ApJ*, 765, 47
 Nestor, D. B., Shapley, A. E., Steidel, C. C., & Siana, B. 2011, *ApJ*, 736, 18
 Oesch, P. A., Bouwens, R. J., Illingworth, G. D., et al. 2014, *ApJ*, 786, 108
 Ono, Y., Ouchi, M., Mobasher, B., et al. 2012, *ApJ*, 744, 83
 Ouchi, M., et al. 2008, *ApJS*, 176, 301
 Pentericci, L., Fontana, A., Vanzella, E., et al. 2011, *ApJ*, 743, 132
 Rauch, M., Haehnelt, M., Bunker, A., et al. 2008, *ApJ*, 681, 856
 Robertson, B. E., & Ellis, R. S. 2012, *ApJ*, 744, 95
 Robertson, B. E., Furlanetto, S. R., Schneider, E., et al. 2013, *ApJ*, 768, 71
 Robertson, B. E., Ellis, R. S., Furlanetto, S. R., & Dunlop, J. S. 2015, *ApJ*, 802, LL19
 Schaerer, D. 2014, *arXiv:1407.2796*
 Schaerer, D., de Barros, S., & Stark, D. P. 2011, *A&A*, 536, A72
 Schenker, M. A., Stark, D. P., Ellis, R. S., et al. 2012, *ApJ*, 744, 179
 Schmidt, K. B., Treu, T., Trenti, M., et al. 2014, *ApJ*, 786, 57
 Shapley, A. E., Steidel, C. C., Pettini, M., & Adelberger, K. L. 2003, *ApJ*, 588, 65
 Shimasaku, K., et al. 2006, *PASJ*, 58, 313
 Stark, D. P., Ellis, R. S., Chiu, K., Ouchi, M., & Bunker, A. 2010, *MNRAS*, 408, 1628
 Stark, D. P., Ellis, R. S., & Ouchi, M. 2011, *ApJ*, 728, LL2
 Stark, D. P., Schenker, M. A., Ellis, R., et al. 2013, *ApJ*, 763, 129
 Takahashi, M. I., et al. 2007, *ApJS*, 172, 456
 Taniguchi, Y., et al. 2007, *ApJS*, 172, 9
 Tilvi, V., Papovich, C., Finkelstein, S. L., et al. 2014, *arXiv:1405.4869*
 Topping, M. W., & Shull, J. M. 2015, *ApJ*, 800, 97
 Treu, T., Schmidt, K. B., Trenti, M., Bradley, L. D., & Stiavelli, M. 2013, *ApJ*, 775, L29

APPENDIX

The line detections shown in Figure 2 have been smoothed with a gaussian kernel of width $\sigma = 1.0 \text{ \AA}$ and are shown centered on the line in an interval of 60 \AA . These choices make it more difficult to judge of the reality of the line with respect to sky noise and its prominence compared to other possible features. To remedy this, we replot in this Appendix the same spectra of Figure 2 for 13 LAEs and 12 [O II]-emitters over the full $\sim 135 \text{ \AA}$ bandpass of the search window, 8115 \AA to 8150 \AA . The smoothing has been reduced to $\sigma = 0.387 \text{ \AA}$ (1 pixel, compared to the instrumental resolution of $\sim 2.5 \text{ \AA}$ FWHM) to show the noise after sky subtraction. The vertical scale for the spectra plotted in black is marked at the bottom left at the level 33 counts per pixel, equivalent to a flux of $1.5 \times 10^{-19} \text{ ergs s}^{-1} \text{ cm}^{-2}$. The stronger spectra plotted in blue are shown at half this scale and marked accordingly.

Figure 5 confirms that these emission-line sources are the same objects found in the 2008 search, by demonstrating that each is the strongest feature in the band of the search. That is, in addition to detecting an emission line within 10 \AA of search detection — as shown in Figure 1, that line is also the strongest feature in the bandpass. Identification of these emission lines with those of the search are based on a coincidence of sky position to $\sim 0.5 \text{ arcsec}$ — the placement of the slit for the confirmation spectrum, the spatial position along the slit to within $\pm 2 \text{ arcsec}$, and to a correspondence of the strongest feature in the confirmation spectra to the predicted wavelength, with a typical agreement of 5 \AA .

Moreover, the identified lines are the only *statistically significant* features in the spectra. We have calculated the signal-to-noise ratio (SNR) of each emission feature using the unsmoothed, sky-subtracted spectra at their raw dispersion of $0.387 \text{ \AA pixel}^{-1}$. For each object we selected the pixels over which the line flux had been measured, marked in Figure 5 by the short red lines. The remaining pixels were used to determine the noise in counts, without removing possible additional sources. (Segments that are set to zero are gaps in the CCD mosaic array.) The SNR for each feature, determined as the square root of the sum of the squares of signal-to-noise calculated pixel by pixel, is recorded next to each feature: each line is a highly significant detection with $\text{SNR} > 6$. These determinations of SNR are in good agreement with those done for the 2008 search data (see Figure 3 of MNS2), which were determined photometrically using the two-dimensional spectral images (“spaxels”). It is clear from inspection of the marked lines and the SNR that no other features are detected over these wavelength intervals at a significance of over 5σ , the standard criterion for a detection in photometric or spectroscopic data.

Returning to the question of source identification discussed in §3.1, we now review the possibility of misidentification of what are clearly real sources. Spectra with multiple, well-spaced lines are clearly not LAEs, so these cases in the right column of Figure 2 have not been replotted Figure 5. Only [O II] can be confused with $\text{Ly}\alpha$. At the full 2.5 \AA FWHM resolution of these spectra, it is clear that the [O II] doublet ($\lambda\lambda 3726, 3729 \text{ \AA}$) can be easily distinguished from $\text{Ly}\alpha$, even in cases of relatively low SNR. Each of the faintest 6 sources identified here as $\text{Ly}\alpha$ have sufficient SNR to distinguish them from [O II] because they do not show any structure with the 5 \AA (redshifted) spacing of the [O II] doublet. We consider the most ambiguous case to be the faintest [O II] emitter, which could be faint $\text{Ly}\alpha$ with a noise spike on the to the blue that has the proper 5 \AA spacing. Judging from the SNR, it appears that this is a possible but unlikely (probability $< 10\%$), similar to the chance that any one of the five faintest $\text{Ly}\alpha$ lines is actually a very noisy [O II].

In summary, inspection and analysis of the spectra of $\text{Ly}\alpha$ candidates at full spectral resolution confirms that, with high probability, the lines recovered in the 2013 & 2014 observations are those found in the 2008 search, and that the discrimination between $\text{Ly}\alpha$ emission and foreground sources is secure.

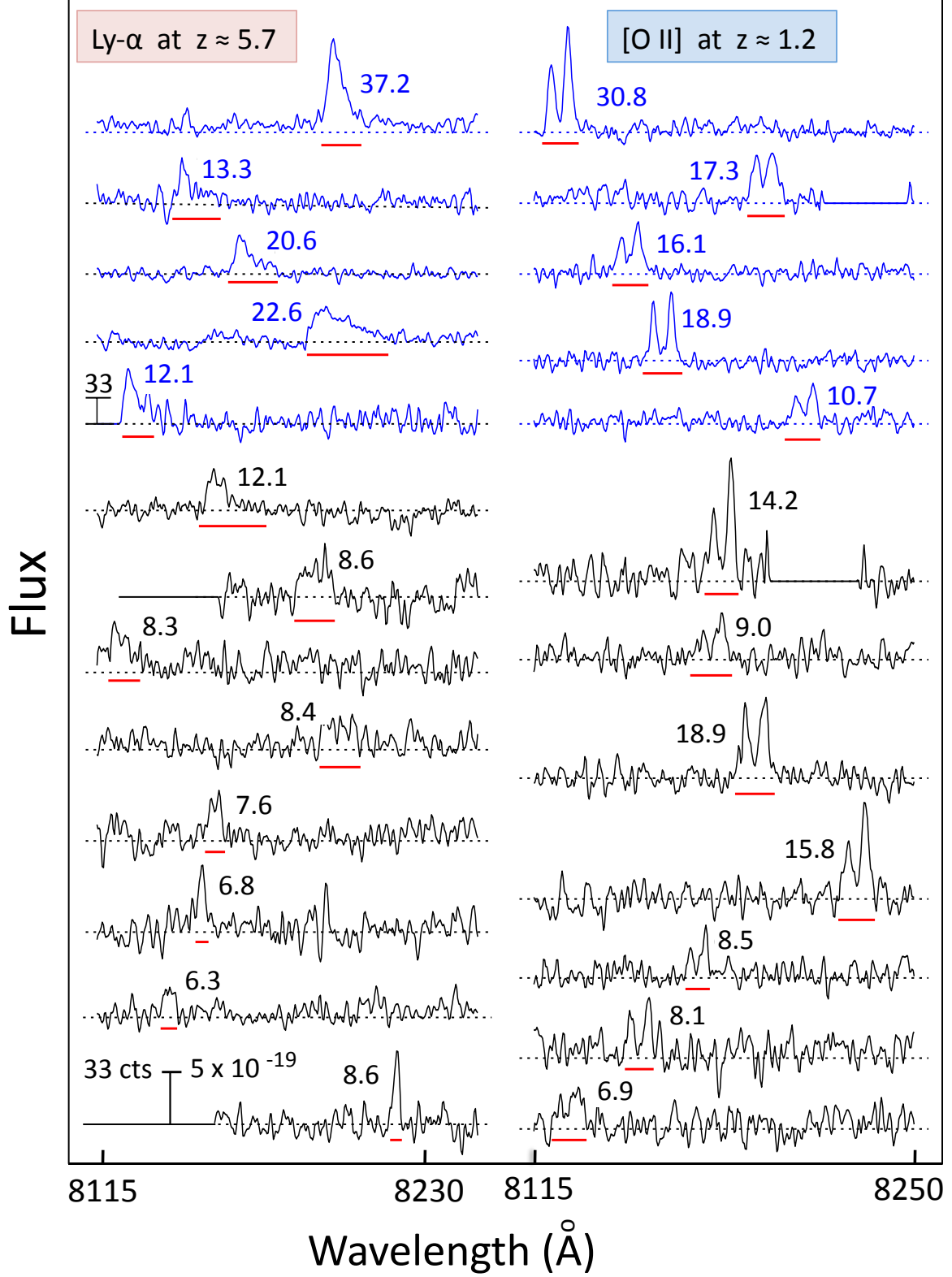


FIG. 5.— Sky-subtracted spectra of identified Ly α lines (left) and foreground [O II]-emitters (right), smoothed with a gaussian kernel of width $\sigma = 1$ pixel (0.387 \AA), and plotted over the full interval of the narrow-band filter, $8115\text{--}8250 \text{ \AA}$. (These are the same objects shown in Figure 2 left and middle columns.) The vertical scale, in counts and equivalent flux ($\text{ergs s}^{-1} \text{ cm}^{-2}$), is shown at the bottom left for spectra in black; the scale of spectra plotted in blue is compressed by a factor of two, as shown (5th from top, left-side). The zero-level of each spectrum is shown as a dashed line; solid flat lines are for chip gaps in the CCD mosaic array. Detected Ly α and [O II] are marked by short red lines. The numbers adjacent to each feature record the SNR of the feature, computed from pixel-by-pixel signal-to-noise, as described above. All features well exceed to customary 5σ criterion for detection.

TABLE 1
IDENTIFIED LAES AT $z = 5.7$

#	Identification	RA (2000.0)	DEC (2000.0)	$\lambda_{\text{Ly}\alpha}$ angstroms	Flux $\times 10^{18}$ ergs s $^{-1}$ cm $^{-2}$	SNR
1	14.5+3-0.91	15:23:00.333	-00:13:28.18	8199	11.5	37.2
2	17.5-2-0.18	15:23:12.900	-00:15:33.56	8196	8.7	13.3
3	54.5+6-0.43	15:23:08.617	-00:01:24.37	8146	7.8	20.6
4	58.5+5-0.94	15:23:18.792	-00:02:31.55	8167	7.0	22.6
5	40.5-4-0.95	15:23:43.210	-00:15:01.20	8127	6.1	12.1
6	31.5+6-0.66	15:22:56.159	-00:06:23.60	8157	5.0	12.1
7	44.5+4-0.54	15:23:12.015	-00:05:46.11	8192	4.6	8.6
8	63.5+8-0.92	15:23:08.087	+00:01:53.87	8121	4.6	8.3
9	13.5+3-0.45	15:22:58.690	-00:13:24.69	8201	4.0	8.4
10	55.5-5-0.43	15:23:57.310	-00:13:16.30	8157	3.5	7.6
11	32.5-2-0.74	15:23:27.052	-00:13:47.32	8147	3.3	6.8
12	46.5-5-0.75	15:23:51.911	-00:15:05.34	8141	2.6	7.3
13	56.5-4-0.68	15:23:53.999	-00:12:04.48	8221	1.9	8.6

TABLE 2
SHIMASAKU ET AL. LAE LF MODELS AND MNS2 LAE LF REALIZATIONS

model LF _{LAE} α, L^*, Φ^*	R_{model} N(-17.6)/N(-17.3)	$R_{\text{realization}}$ N(-17.6)/N(-17.3)	[O II]	Foreground LF parameters [O III]	H α
-1.0, 42.72, -2.92	1.621	1.628	[-1.44, 41.47, 0.768]	[-1.69, 41.42, -0.172]	[-1.69, 41.49, -1.392]
-1.5, 42.90, -3.20	1.895	1.891	[-1.39, 41.52, 0.790]	[-1.68, 41.42, -0.063]	[-1.67, 41.49, -1.287]
-2.0, 43.20, -3.80	2.284	2.286	[-1.30, 41.48, 0.836]	[-1.60, 41.42, -0.017]	[-1.60, 41.49, -1.303]

NOTE. — (1) LF_{LAE} Schechter function parameters from Shimasaku et al. (2006); (2) ratio of integrated LAE counts, $N(\log F > -17.6 \text{ ergs s}^{-1} \text{ cm}^{-2})/N(\log F > -17.3 \text{ ergs s}^{-1} \text{ cm}^{-2})$, for Shimasaku et al. model, and (3) for MNS2 data realization; (4) Foreground LFs: Schechter parameters [α , $\log L^*$, $\log \Phi^*$]

TABLE 3
LF FUNCTION FITS AND PROBABILITIES

model LF _{LAE} α, L^*, Φ^*	R_{model}	$R_{\text{realization}}$	[O II] LF α, L^*, Φ^*	[O III] LF α, L^*, Φ^*	LAE fraction	LAEs	Monte Carlo $n = 13$	Probability %
-1.0, 42.72, -2.92	1.621	1.628	-1.44, 41.47, 0.768	-1.69, 41.42, -0.172	0.099	4.0	1.0E-4	0.01%
-1.5, 42.90, -3.20	1.895	1.891	-1.39, 41.52, 0.790	-1.68, 41.42, -0.063	0.142	5.7	1.9E-3	0.19%
-1.6, 42.95, -3.30	1.959	1.957	-1.38, 41.48, 0.796	-1.65, 41.42, -0.057	0.151	6.0	3.2E-3	0.32%
-1.7, 43.01, -3.40	2.029	2.027	-1.37, 41.48, 0.804	-1.64, 41.42, -0.049	0.177	7.1	0.015	1.5%
-1.8, 43.07, -3.52	2.105	2.107	-1.35, 41.48, 0.812	-1.62, 41.42, -0.041	0.198	7.9	0.039	3.9%
-1.9, 43.13, -3.65	2.171	2.171	-1.34, 41.48, 0.822	-1.64, 41.42, -0.031	0.218	8.7	0.076	7.6%
-2.0, 43.20, -3.80	2.284	2.286	-1.30, 41.48, 0.836	-1.60, 41.42, -0.017	0.260	10.4	0.224	22%
-2.1, 43.28, -3.95	2.392	2.391	-1.21, 41.41, 0.754	-1.58, 41.36, 0.063	0.285	11.4	0.345	35%
-2.2, 43.36, -4.12	2.506	2.508	-1.17, 41.41, 0.756	-1.55, 41.36, 0.081	0.302	12.1	0.550	45%
-2.3, 43.45, -4.30	2.637	2.639	-1.16, 41.41, 0.712	-1.47, 41.36, 0.115	0.363	14.5	0.741	26%
-2.4, 43.54, -4.50	2.783	2.781	-1.11, 41.41, 0.680	-1.40, 41.36, 0.147	0.416	16.6	0.907	9.1%
-2.5, 43.63, -4.71	2.944	2.944	-1.05, 41.38, 0.593	-1.18, 41.34, 0.236	0.477	19.1	0.981	2.0%

NOTE. — (1) LF_{LAE} Schechter function parameters based on Shimasaku et al. (2006); (2) ratio of integrated LAE counts, $N(\log F > -17.6 \text{ ergs s}^{-1} \text{ cm}^{-2})/N(\log F > -17.3 \text{ ergs s}^{-1} \text{ cm}^{-2})$ for Shimasaku et al. model, and (3) for MNS2 data realization; (4) LF [O II] Schechter function parameters; (5) LF [O III] Schechter function parameters; (6) predicted LAE fraction, LAE/(LAE+fore), over flux interval $-17.6 > \log F > -17.3$; (7) expected number of LAEs; (8) fraction of cases in Monte Carlo test with 13 LAEs and 27 foreground galaxies; (9) Probability of LF_{LAE} slope α .